# Populations and coherence in femtosecond time resolved X-ray crystallography of the Photoactive Yellow Protein

Christopher Hutchison[1] and Jasper J. van Thor*[1]

1. Imperial College London, Molecular Biophysics, Sir Ernst Chain Bld. South Kensington Campus. LondonSW7 2AZ, UK

*Corresponding author e-mail j.vanthor@imperial.ac.uk

Abstract

Ultrafast X-ray crystallography of the Photoactive Yellow Protein with femtosecond delays using an X-ray Free Electron Laser has successfully probed the dynamics of an early Franck-Condon species. The femtosecond pump-probe application of protein crystallography represents a new experimental regime that provides an X-ray structural probe for coherent processes that were previously accessible primarily using ultrafast spectroscopy. We address how the optical regime of the visible pump, that is necessary to successfully resolve ultrafast structural differences, affects the motions that are measured using the technique. The sub-picosecond photochemical dynamics in PYP involves evolution of a mixture of electronic ground and excited state populations. Additionally, within the dephasing time structural motion include vibrational coherence arising from excited states, the ground state and a ground state intermediate under experimental conditions used for ultrafast crystallography. Intense optical pulses are required to convert population levels in PYP crystals that allow detection by X-ray crystallography, but the compromise currently needed for the optical bandwidth and power has consequences with regard to the contributions to the motions that are experimentally measured with femtosecond delays. We briefly review the ultrafast spectroscopy literature of the primary photoreactions of PYP and discuss relevant physical models taken from coherent control and femtosecond coherence spectroscopy literature that address both the population transfer as well

as the vibrational coherences. We apply linear response theory, with the additional use of a high power approximation, of on-resonance impulsive vibrational coherence in the ground state and the non-impulsive coherence in the excited state and discuss experimental approaches to manipulate the coherence contributions. The results are generalised and extended to discuss the future capabilities of high repetition rate XFEL instruments providing enhanced sensitivity to perform the crystallographic equivalent of an impulsive Raman measurement of vibrational coherence.

## *1. Introduction - Time resolved structural measurements of the Photoactive Yellow Protein by X-ray crystallography*

X-ray Free Electron Lasers (XFELs) are novel instruments that provide the capability to conduct time resolved X-ray crystallography experiments with femtosecond time resolution. It is anticipated that the high repetition rate combined with a potential for increased time resolution and sensitivity of the European XFEL instrument will allow experimental access to high frequency, low amplitude vibrational coherence in protein crystals. Ultrafast protein X-ray crystallography was first developed at third generation light sources, but the experimental implementation at XFELs and the ability to access coherent processes is essentially different.
The Photoactive Yellow Protein (PYP) was one of the first light-sensitive proteins to be used for time-resolved pump-probe X-ray crystallography, initially by the TR-Laue method [1–7]. Using synchrotron sources, a time resolution for TR-Laue of up to 100 ps is possible, and several groups have reported on sub-nanosecond measurements and slower time scales [1,2]. The PYP has become a model to study protein structural dynamics over many decades of time, having been observed from sub-nanoseconds to seconds at synchrotrons. These successes were also enabled by a combination of several properties of PYP crystals. Firstly, hexagonal PYP

crystals readily diffract to high resolution, providing near-atomic resolution information. Second, the mosaic spread of PYP crystals is very small, typically less than 0.05 degrees, which favours accurate integration of Laue patterns and high quality Laue crystallography. Third, nanosecond excitation generates detectable levels of photointermediates following photoisomerisation with considerable optical penetration depth that also matches the currently possible spot size of the polychromatic X-rays at Laue stations such as APS/14ID and ESRF/ID09B. By stretching the optical pulse beyond the picosecond excited state lifetime, accumulation of photoproducts under this quasi-continuous wave regime may in principle exceed the primary quantum yield, estimated at ~20% [8]. Fourth, photoproducts are fully isomorphous with ground state and remain so for the duration of the full photocycle. Furthermore, diffraction quality in terms of resolution, mosaicity and merging statistics is not significantly affected by optical pumping, although multiple pump-probe cycles are avoided. Few light-sensitive protein crystals satisfy each of these important criteria, establishing the PYP in addition to the myoglobin-CO complex as most amenable to time resolved X-ray crystallography.

Based on very similar data, different interpretations have also been argued, in particular with regard to the chromophore conformation of the early, 100 ps, PYP structure, but also to propose different reaction schemes for nanosecond and microsecond intermediates [1,2]. Regarding the early, sub-nanosecond, chromophore structure, discussion has focussed on the chromophore dihedral angle C1-C2-C3-C1'. In one study, this dihedral angle was found by X-ray structural refinement with application of Density Functional Theory (DFT) derived structural restraints to have a value of 33 degrees in the '$pR_0$' structure at 100 ps (4B9O pdb [2]) Jung et al. used structure refinement avoiding additional restraints to arrive at a structure with a 90 degree dihedral angle for the '$I_T$' state (4I38 pdb [1]) (corresponding to the '$pR_0$' in 4B9O pdb [9]).

In contrast, Schotte et al. [2] and Kaila et al. [10] argue on the basis of DFT calculations that the structure should be closer to having a 33 degree dihedral angle.

A second fundamental difference between both papers concerns the bifurcation which is proposed by Jung et al. from the first IT state to form the '$pR_1$ and '$I_{TC}$' states with 3 ns and 1.7 ns, respectively (Jung et al. [1], figure 1a). The $I_{TC}$ state further decays in 20 ns to form a $pR_2$ state, such that delays from 50 ns typically show a product state that is a mixture of $pR_1$ and $pR_2$ where the phenol rings have different orientations (the '$pR_1$' species corresponding to the phenol position that is eventually developed in the long-lived millisecond intermediate 'pB'). Jung et al. further observed that in the E46Q mutant this bifurcation does not occur and only the $pR_1$ intermediate is populated. In contrast, Schotte et al. report only one species in the nanosecond range (assigned '$pR_1$' in Schotte et al. [2]). Considering that these opposing conclusions were drawn on the basis of similar quality TR-Laue data, future experimental contributions could help by providing even better resolved time resolved data. Recent TR-SFX experiments with either nanosecond excitation or femtosecond excitation however supported the presence of a mixture of cis-like and trans-like chromophore structures with 200ns pump-probe delay [11,12]. Particularly, the processing statistics and magnitude of the signal-to-noise of the electron density maps may determine whether a second conformation can be supported in the nanosecond regime. It was previously shown that a nanosecond time resolved serial femtosecond crystallography experiment of PYP microcrystals retrieved difference electron density signals with very good sensitivity mainly because of the much increased levels of photolysis that is possible with the small optical penetration and nanosecond excitation [11]. These earlier measurements did not have the time resolution to directly probe the trans-cis photoisomerisation reaction of the p-coumaric acid chromophore, which proceeds with a time-

constant of approximately 500 fs [8,12], while more recent work achieved this with an effective experimental bandwidth of 3.15 THz [13].

It was shown that nanosecond excitation of the PYP readily produced detectable electron density differences using the Serial Femtosecond Crystallography technique (SFX) using an X-ray Free Electron Laser [11]. Using a Monte-Carlo integration approach for SFX diffraction data is known to result in data-sets that have relatively moderate signal-to-noise ($I/\sigma I$), having typical values of 6 for processing of 400,000 images of PYP, in space group $P6_3$ [11]. However the internal R-factor 'R-split' can be very good for such data (given as 14% for the 400,000 images mentioned above). It is noted that very strong electron density differences were retrieved also where the 'light' data was reduced to an R-split value of 20% [11]. Moreover, an important consideration for the accurate retrieval of photoinduced structure factor differences $\Delta F$ is that the SFX method generates data where the pumped and the un-pumped diffraction is highly isomorphous. Because each exposure is a fresh crystal, and the femtosecond pulse duration records mostly radiation damage free diffraction [14–16], there are no cumulative background contributions to the difference measurement. In contrast, synchrotron-based time resolved Laue diffraction typically 'fills' the full dynamic range of the detector in multiple pump-probe cycles that causes X-ray and laser damage to contribute as background. The success of the nanosecond TR-SFX study of PYP was further aided by the much reduced optical penetration depth that is probed in microcrystals, which maximises photolysis if the pulse duration far exceeds the excited state lifetime. Indeed, achieving more than 50% conversion with nanosecond pulses maximised the magnitude of the difference electron density significantly [11].

Using the SFX technique with femtosecond visible excitation, it was recently shown that motions of the p-coumaric acid chromophore and the protein could be recorded to probe the early Franck Condon state with femtosecond delays [12]. Under optical conditions that optimised the population transfer to the '$I_0$' product state via $S_1$, and suppressed non-linear processes by addition of controlled amounts of second order and third order dispersion, detectable levels of pumped intermediate could be generated [12,17]. The visible pulse duration was 140 fs and allowed observation of Franck Condon motion which rapidly dominated the difference maps. It was estimated from the diffraction data of a 200 ns pump-probe delay that approximately 10% was converted by the femtosecond optical pulse [12]. Differences of the chromophore structure were observed already at ~150 fs. It is noted that the determination of time-zero which is subsequently used for the calibration of the arrival time which is recorded for each XFEL pulse using the timing tool relies on a cross-correlation measurement of transient reflectivity in a Ce:YAG scintillation screen. The group velocity mismatch for 60 microns 1/e penetration depth at 10 KeV together with <100 fs additional delay contribution from secondary ionisation to the transient reflectivity add some uncertainty to the time-zero determination, but may be modelled to within the experimental bandwidth. Independently, the presence of pump-probe differences in the earliest time bins, as well as the duration of trans-cis isomerisation, agreed well with the time-zero determination (figure 2). At ~150 fs, an out-of-plane motion of the C1-C2-C3 part of the chromophore had already titled the phenol ring away from its ground state conformation (figure 2). Analysis of short-time bins of the sub-ps data indicated a characteristic transition time at ~600 fs, closely matching the reported photoisomerisation time constant under comparable conditions [8] (figure 2). At 3 ps the out-of-plane distortion is complete and was assigned to the primary photoproduct '$I_0$'. As discussed below and in Pande et al. [12], the majority of these difference electron density signals is argued to belong to the Franck Condon motion, whereas vibrational coherence must

also contribute to pump-probe delays within the dephasing time. A detailed description of the chromophore conformation in the $I_0$ state, and refined values for the available pump-probe time delays is presented in Table S3 of Pande et al. [12] Notably, the characteristic dihedral angle C1-C2=C3-C1' was refined at a value of 140, 30 and 38 degrees at 269 fs, 940 fs and 3 ps, which compares to a value of 172 for the ground state. Interestingly, the 3 ps conformation of the dihedral angle C1-C2=C3-C1' compares more closely with the '$pR_0$' structure at a 100 ps delay (4B9O pdb [2]) rather than the '$I_T$' structure at 100 ps delay reported by Jung et al. (4I38 pdb [1]) (figure 3).

The time dependence of both the difference electron density and refined chromophore dihedral angle C1-C2=C3-C1' from extrapolated maps indicated the presence of a ~550 fs 'dwell' time, while the transition time was seen to correspond to the bandwidth-limited rate [12]. It was consequently proposed that the phase imparted by the optical pump is maintained for the duration of this dwell-time, corresponding to coherent nuclear motion. The presence of the dwell time observed from TR-SFX is in good agreement with femtosecond Stimulated Raman measurements of PYP, as discussed in section 2 below.

### *2. Primary photochemical reactions and coherence of PYP*

The time-constant for photoisomerisation of the PYP chromophore has been reported with values ranging from ~400 fs to 1.4 ps, depending on the details of optical conditions and spectroscopic probe, and also sample conditions [19–22]. Notably, excited state decay has been shown to be multi-phasic from femtosecond fluorescence and transient absorption

spectroscopy [8,20]. It is also well established that excited state population that persists for picoseconds is unproductive in the formation of the cis-like photoproduct $I_0$, and photoisomerisation proceeds with a dominant time constant of ~600 fs [8,22,23]. The isomerisation time constant and excited state life-times are of particular interest since these may determine if excited state coherent motion may persist to the point of isomerisation. Typically, vibrational dephasing times in proteins are on the order of ~1 ps [24], and femtosecond fluorescence upconversion experiments of PYP have detected vibrational coherence persisting up to ~1.5 ps [25,26]. Mataga et al. found that the frequency and damping times of excited state vibrational coherence were mostly independent of excitation wavelength between 480 nm and 550 nm. Generally, modes at ~140 $cm^{-1}$ and 50 $cm^{-1}$ were observed with characteristic damping times of ~700 fs and ~500 fs [25]. In addition to differences in the reported excited state lifetime of PYP, values for the primary quantum yield of photoisomerisation range from 0.14 [8] to 0.55 [27]. These variations can partly be explained from different methods and analysis that was used, but it has been emphasized that the optical conditions for femtosecond spectroscopy measurements will significantly contribute [8]. The long-lived vibrational coherence from fluorescence measurements does not report on the isomerisation coordinate which is not vibronic. Instead, it has been pointed out that near-harmonic and symmetric modes selectively contribute to the time resolved fluorescence. Also, the ultrafast spectroscopy literature generally describes the photoisomerisation of the PYP chromophore as an incoherent rate process with exponential decays. This description appears to be at odds with the analysis of the chromophore reaction coordinate that is shown in figure 2. The presence of a femtosecond ‘dwell’ time together with a transition time that fits the experimental bandwidth, which was 3.15 THz, resembles a delayed ballistic event. Rate kinetics would require this transition time to be stretched corresponding to the duration of the dwell time, which is not seen in the time resolved crystallographic experiments. The present

analysis thus assumes that the ensemble phase relation resulting from the optical pulse is maintained in this description up to the transition time. This does however not constitute evidence for a coherent reaction coordinate, such as seen on considerably faster timescale in photoisomerisation of rhodopsin from transient grating spectroscopy [28]. Future experimental investigations may revisit this observation in PYP, applying for example multi-pulse pump-dump-probe experiments. While the question of possible coherence contribution to isomerisation of PYP is of interest, here we focus instead on the physical assignment and optical control of displacements that are measured in a femtosecond TR-SFX experiment in general, and in PYP in particular.

A number of femtosecond visible transient absorption studies have characterised the fs and ps dynamics of PYP, which are reviewed and summarised elsewhere [8,29,30]. In order to consider models that describe the femtosecond and picosecond populations in PYP we highlight two particular experimental observations. Firstly, it was discovered that even weak femtosecond excitation at 400 nm in the blue edge of the ground state absorption band ($I_{max}$ = 446 nm) results in significantly different transient absorption changes as compared to on-resonance or red-edge excitation [23]. Larsen et al. [23] showed that photoionisation occurs with blue excitation and studied the power dependence of the transient absorption belonging to the chromophore radical at 370 nm and red electron absorption due to the solvated ejected electron between 550 nm and 650 nm. Lincoln et al. [8] quantified these processes for stretched pulses at 400 nm, 450 nm and 490 nm with addition of positive dispersion and found that even with on-resonance excitation some evidence for contribution of the photoionisation pathway was evident [8]. The photoionisation pathway is therefore one of the loss-channels which must be minimised when crystals are pumped with intense pulses the aim to maximise conversion.

Second, transient visible absorption as well as transient mid-IR absorption has revealed the presence of an early intermediate which has been assigned to an electronic ground state species [19,23,30]. This ground state intermediate (GSI) is characterised by distinctive induced absorption at 490 nm, while the primary photoproduct absorbs maximally at ~510 nm [23,30]. Furthermore, the GSI shows further well resolved induced absorption, albeit with smaller amplitude, in the 520 nm – 620 nm region which was previously unreported [8]. It has been concluded that in the wild type the yields of formation of the GSI and the photoproduct $I_0$ are approximately equal at ~30% (figure 4a) [23,29]. It is emphasized that the transient concentration of the GSI is sensitive to the optical parameters [8], and it has been argued on the basis of transient absorption spectroscopy [8] done under comparable optical conditions that femtosecond and picosecond delays of the recent TR-SFX study should include only small contributions from the GSI [12]. An alternative modelling of ultrafast measurements, using infrared detection, assumed that all population resulting in ground-state re-filling passes through the GSI, which represents 72% of the total decay amplitude [19]. However based on the amplitude of the distinguishing transient absorption at 490 nm, the assumption of nearly equal branching between direct ground state recovery and passage through the GSI is more probable (figure 4c) [8,29]. There is still considerable speculation with regard to the nature and also the structure of the GSI. Van Wilderen et al. [19] retrieved the IR difference spectrum for the GSI in the 1800-1200 $cm^{-1}$ spectral window using ultrafast infrared spectroscopy, and assigned a ~70% yield for its formation. Global analysis separated the spectra for the excited state decay (1.2 ps in their measurement) and the GSI decay (6.2 ps) which did show distinct similarities but also some differences. For instance in measurements of the E46Q mutant, induced absorption near ~1470 $cm^{-1}$ is prominent in both ES and GSI spectra, as is induced absorption at 1695 $cm^{-1}$. While on the basis of the IR spectra it may not be obvious that the GSI has a ground state electronic configuration, this argument is mostly developed on the basis

of pump-dump-probe experiments [23,30]. Larsen et al. showed that by dumping at either 500 fs and 2 ps with a 505 nm pulse, population inversion caused the induced absorption particularly at 480 nm and 490 nm where the GSI absorbs [23,30]. Van Wilderen et al. argued that both the excited state decay spectrum and the GSI spectrum lack a band at 1667 $cm^{-1}$ which appears in the $I_0$ (and also I1) state of the E46Q measurements. This mode has been assigned to the chromophore C=O group after it has reconfigured to break the interaction with the N backbone atom of Cys-69 [26]. From this observation it may be concluded that the chromophore C=O group should be in the same position as in the excited state [19]. An X-ray crystallographic measurement may therefore potentially not distinguish the chromophore conformations in the $S_1$ and GSI states [12]. However van Wilderen et al. noted that a weak ground state bleach in the GSI spectrum at 1638 $cm^{-1}$ assigned to the central ethylenic C=C bond may indicate modification and potentially isomerisation of the chromophore [19,29]. Figure 4 (below) summarises the general schemes for primary photochemical reactions of PYP. The middle and right figure expand on the generally accepted view of a branching between GSI and $I_0$ formation to include inhomogeneous and alternatively homogeneous models of multiphasic dynamics.

Stahl et al. [29] investigated the branching yield of modified PYP samples, which incorporated a ‘locked’ chromophore analog 5-hydroxy indan-(1E)-ylideneacetic acid in which single bond rotation C3-C1’ is prevented. In these samples it was found state excited state decay was faster with a 700 fs time constant, and that the transient population of the GSI was approximately doubled showing a 79% yield. Nevertheless photoisomerisation results in a reduced level of $I_0$, but this smaller population subsequently launches a functional photocycle. Stahl et al. thus argued that single bond rotation of C3-C1’ is not an alternative to C2=C3 double bond rotation but appears to enhance the photoisomerisation quantum yield. This view appears to fit with

recent femtosecond time resolved X-ray crystallography which showed a dominant transition at 550 fs that involves both C2=C3 double bond rotation and C3-C1' single bond rotation [12]. With regard to the C1=O1 position, Pande et al. showed that already at early delays (maps presented at 269 fs) the distance from the pCA-O1 to cys69-N had increased to 3.05 Å , from 2.77 Å in the ground state. At 3 ps this distance was 3.12 Å. This suggests that the electron density differences that dominate the sub-picosecond measurements should correspond to population that is expected to visibly modify the frequency of the chromophore C1=O1 stretching vibration [19]. While spectroscopy shows that with delays shorter than 500 fs the population should predominantly be excited states, with some GSI appearing, it is reasonable to propose an assignment of transient electron density signals to Franck-Condon motion [12]. Ultrafast spectroscopy literature is in good agreement with the time-dependence of the dynamics observed in the ultrafast X-ray crystallography. In particular, ultrafast vibrational spectroscopy of PYP has established the chromophore response on ultrafast time scale. Creelman et al. [31] observed using femtosecond stimulated Raman spectroscopy a Franck-Condon intermediate already at ~100 fs, distinct from the major $S_1$ decay process with a ~450 fs time constant. The FC state already showed gained intensity of a 958 $cm^{-1}$ Hydrogen-out-of-plane (HOOP) mode, indicative of chromophore distortion at the ethylenic C2=C3 [31]. This assignment appears to be in excellent agreement with the TR-SFX structures with pump-probe delays shorter than ~600 fs [12].The decay of this Franck-Condon state with a ~170 fs time constant agrees reasonably well with the structural motions seen in the TR-SFX experiment prior to excited state decay, occurring with ~500 fs 'transition time'. Furthermore, the $C_1$=$O_1$ carbonyl out-of-plane vibration downshifts from 665 to 640 $cm^{-1}$ concurrent with excited state decay which was interpreted as resulting from motion along the photoisomerisation coordinate [31]. The correspondence between X-ray structural and Raman structural measurements of Franck-Condon motions in PYP also highlights that selection rules

must be considered for each ultrafast observation. The X-ray crystallographic ensemble measurement of ultrafast electron density differences, which are detected primarily from the high-resolution information, is determined by the scattering cross sections, magnitude of real-space displacements, Debye-Waller factors and temperature, population levels, static and dynamic site disorder and is strongly affected by signal-to-noise ($I/\sigma I$) of the structure factor difference measurement. Ultrafast spectroscopy add the specific selection rules and do not detect real-space displacement directly, yet decades of Raman spectroscopy has developed advanced theory that is applicable to evaluate the magnitude of vibrational coherence under representative optical conditions. While most of this work is developed to express the nonlinear optical susceptibility, the connection to real-space displacement is considered in the sections 4) and 5).

### *3. Optical control of population transfer in PYP*

Under conditions of weak illumination, or nanosecond excitation as used in Tenboer et al. [11], the optical penetration depth is determined by the ground state cross section of the PYP chromophore, while the photolysed yield may in principle reach levels that are several times the primary quantum yield at high pulse intensities by virtue of stretching the pulse duration far beyond the ~500 fs excited state lifetime. In contrast, the penetration depth under intense femtosecond optical excitation will be dominated by non-linear cross sections, while the photolysed yield becomes fundamentally limited by the primary quantum yield of photoisomerisation of the p-coumaric acid chromophore of PYP. Even if very intense, optical pulses with very short duration (for example below 10 fs) will create only small population levels, either in dilute solution, in micro-crystals or in the synchrotron geometry. Detection of such small populations may be possible in the future employing high repetition rate

measurements at the European XFEL. Rather, approaches to achieve suppression of the non-linear cross sections by manipulation of amplitude and phase of the optical field and carrier frequency selection will aid the design of experimental conditions to allow detection by femtosecond time resolved pump-probe TR-SFX. Such modifications may degrade the achievable time resolution but are specific to the primary photochemical dynamics of the system under study. Phenomenologically, at a center wavelength of 450 nm and 300 fs pulse duration, addition of +5,000 $fs^2$ second order dispersion and using 46.7 GW $cm^{-2}$ power, the primary product formation approached ~20% in solutions of PYP while optical penetration in crystal would be expected to extend to ~40 μm based on the suppressed nonlinear cross sections found using the Z-scan technique and also from global analysis of femtosecond transient absorption measurements [8]. In order to evaluate the effective stimulated emission cross section at wavelengths near at 450 nm and varying pulse duration and chirp, the time constant for the dynamic Stokes shift is of importance which was found to be very fast and less than 200 fs [21].

There are indications from spectroscopy measurements that the primary photochemical processes in PYP crystals may differ from those occurring in solutions [17]. Currently there is no reliable measurement of the excited state lifetime in PYP crystals, but recent flash photolysis measurements using characterized femtosecond optical pulses of photocycle intermediates has provided an estimate of the primary quantum yield of about 20% [17]. While transient populations of the long-lived pB state up to 10% were determined, the value of the primary quantum yield was taken to be twice this value at 20% [17]. This followed prior crystal spectroscopy measurements of PYP which showed approximately half the population returning back to the ground state after the initial pR formation but before pB formation [32]. Importantly, the power density dependence showed that contributing photobleaching processes

following double excitation can be mostly avoided by seeking the best compromise between power density, hence pulse duration, and resulting photocycle and photobleaching yields. The effective non-linear cross sections and resulting populations under representative optical conditions used for TR-SFX have been determined for femtosecond excitation of crystalline PYP. Strikingly, it was found that there were no significant differences in the total nonlinear cross section with regard to the energy density for 130, 550 and 850 fs pulses [17], in contrast to measurements of PYP in solution [8]. However, the $S_2$ driven photobleaching reactions were seen to be significantly affected instead [17]. The prior observation does indicate that the more viscous crystal environment modifies the ultrafast dynamics and concordantly the cross sections that were measured. The latter result demonstrates that in the case of PYP crystals, even under conditions of resonant excitation, the multi-photon bleaching reactions place the fundamental limits on the pulse duration and power, in light of the population differences that may be generated. It was shown to be possible to convert between 5% and 10% of the interaction region for micro-crystals conditions, but accepting some levels of photo-destruction under conditions that are currently suitable for TR-SFX of PYP. Indeed, femtosecond time resolved TR-SFX performed under controlled optical conditions successfully resolved photochemical processes that are dominated by population of $S_1$ [12].

The question of controlling femtosecond population transfer provides motivation for further optimisation using active pulse shaping methods. Taking approaches from strong field coherent control, considering the frequency-resolved ‘Brumer Shapiro’ scheme [33,34], Optimal Control Theory [35,36] or the time-resolved (pump-dump) ‘Tannor-Rice’ scheme [37], these all provide means for explicit evaluation of spectral phase and specifically second order dispersion and treat wavepacket coherence. The application of chirped pulses to shape nuclear wave packets and enhance or suppress vibrational coherence was developed by

Ruhman and Kosloff [38]. Coherent control with an order of magnitude enhancement has been seen in a case that applied controlled second order dispersion [39]. The experimental ability to achieve high resolution active amplitude and phase shaping of femtosecond pulses has also led to the application of arbitrary search algorithms that use experimental feedback as fitness parameters to arrive at very complex pulses [40]. A pragmatic approach to active pulse shaping would achieve maximum population transfer within a set pulse envelope limit, as an optimization technique for femtosecond time resolved pump-probe TR-SFX. A more systematic approach follows methods already presented [8,17], which determine non-linear cross sections and yields under optical conditions where simple pulse shapes are manipulated by variation of spectral phase, carrier frequency, bandwidth, peak power and pulse duration.

The methodology would need to be extended to include the interference arising from the phase velocity differential and orthogonality between the ordinary and extraordinary directions in the monoaxial PYP crystals, which are in the $P6_3$ hexagonal space group. The refractive index of protein crystals is typically close to 1.5 but at resonance the birefringence will strongly depend on the precise carrier frequency because of anomalous refractive index dispersion differences, as will therefore be the intrinsic birefringence that generally maximizes at the high-frequency edge of resonance. A relatively large intrinsic birefringence is expected for PYP crystals because the dichroism is large; extinction coefficients differ several-fold for the ordinary ($E_1$) and extraordinary ($E_2$) directions. The PYP crystals are uniaxial, with the ordinary wave which has direction perpendicular to the c-axis, where the absorption is:

$$A_1 = \frac{1}{2}\sum_{\alpha} 3\epsilon_{\alpha} cd \frac{1}{m}\sum_{j=1}^{m}\left[1 - \left(\hat{\mu}_{\alpha j}\cdot\hat{\mu}\right)^2\right] \quad (1)$$

Depends only on the angle $\hat{\mu}_{\alpha j}$ of the transition dipole moment with the c-axis.

The extraordinary direction is parallel to the c-axis with absorbance

$$A_2 = \sum_{\alpha} 3\epsilon_{\alpha} cd \frac{1}{m} \sum_{j=1}^{m} \left(\hat{\mu}_{\alpha j} \cdot \hat{\mu}\right)^2 \quad (2)$$

This is proven from the general case for uniaxial crystals

$$\langle (\hat{\mu} \cdot \hat{e})^2 \rangle = \frac{1}{2n} \sin^2\theta \left[ n + \cos 2\phi \sum_{k=1}^{n} cos \frac{4\pi k}{n} - \sin 2\phi \sum_{k=1}^{n} \sin \frac{4\pi k}{n} \right] \quad (3)$$

Where for $n \geq 3$ [41]

$$\langle (\hat{\mu} \cdot \hat{e})^2 \rangle = \frac{1}{2} \sin^2\theta = \frac{1}{2} (1 - (\hat{\mu} \cdot \hat{u})^2) \quad (4)$$

The calculation then gives: $A_1$ = 0.80 and $A_2$ = 0.20. This is experimentally also seen: $A_1$=0.82 and $A_2$=0.18 [42]. The experimentally determined extinction coefficients are in very close agreement to the calculation at $E_1$ (450 nm) = 65 $mM^{-1}$ $cm^{-1}$ (0.82 / 2 μm) $E_2$ (450 nm) = 12 $mM^{-1}$ $cm^{-1}$ (0.15 / 2 μm).

Polarised laser excitation of PYP crystals will for directions excluding those precisely in the $E_1$ or $E_2$ directions result in elliptical polarisation. For linearly polarised light, each different orientation will generate different ellipticity where the perpendicular amplitudes (e1 and e2) are proportional to the inner products E.e1 and E.e2. For circularly polarised light for almost all crystal orientations the inner products E.e1 and E.e2 are expected to be equal such that ellipticity is more invariant. Values for the intrinsic birefringence are not readily available, although estimates may be made based on those for myoglobin crystals [43]. Figure 5 presents the resulting phase difference for micrometre length scale optical propagation. It is seen that

for values of the intrinsic birefringence exceeding $\Delta n=0.01$, which are possible near resonance frequencies, the phase differential becomes significant.

### *4. Vibrational coherence contributions with femtosecond optical pumping of PYP crystals*

How do the optical pulse parameters determine what is measured with a femtosecond pump-probe TR-SFX experiment? With the required intensity and pulse duration it is presently unavoidable to generate contributions from the electronic ground state, in addition to excited state processes. As summarised and demonstrated by calculation below, pulse intensity, carrier frequency and laser bandwidth are primarily responsible for ground state vibrational coherence amplitude contributions. Excited state coherence amplitudes, which are displacement-driven, can be shown to dominate those from the ground state, that are impulsively driven only if pulses are weak, are directly on resonance and/or have very broad or very narrow spectral width compared to the lineshape function. These principles guide future experiments to manipulate vibrational coherence contributions detected by ultrafast crystallography.

Motions of early delays before dephasing, particularly before ~500 fs, result from the contributions of multiple vibrational coherences, have different initial phases, different mode displacements and frequencies, and have both ground and electronic state origins. Those early delay measurements can have significant contributions from an early Franck-Condon state [31], but must also have contribution from electronic ground state vibrational coherence. No clear recurrence was seen for any motion, or difference electron density feature, in the sub-ps and ps TR-SFX difference electron density of PYP [12], but an oscillatory behaviour is not

necessary for complex vibrational coherence motion that is expected. Specifically, a number of ground state and excited state modes, that fit the 3.15 THz bandwidth, evolve under different initial phase and different frequencies. The resulting superposition of the displacements are therefore expected to be complex and simple oscillatory behaviour may not necessarily be detected crystallographically. The existence of vibrational coherence could potentially be expected from ultrafast spectroscopy measurements. For instance, the 50 $cm^{-1}$ and 150 $cm^{-1}$ modes [20] observed in ultrafast fluorescence measurements of PYP correspond to 667 fs and 222 fs periods, respectively. The 50 $cm^{-1}$ mode belonging to the excited state fits the 3.15 THz experimental bandwidth of Pande et al. [12], but were not specifically observed in the X-ray data. The ultrafast spectroscopy measurements however add the Raman selection rules, and the picometre level displacements may not have been resolved at the accuracy obtained. This contrasts with X-ray crystallographic observation of displacement and the isomerisation coordinate is not vibronic. As discussed, the magnitude of the electron difference density is determined by the scattering cross sections of the moving atoms, their Debye-Waller factors and distance of motion. No additional selection rule filters the observations of the resulting displacements, although the spectral density selects the modes.

While the initial amplitudes of excited state and ground state coherence may be comparable, the initial phases for on-resonance pumping are 0 or $\pi$, and $\pi/2$ for the excited state and ground state modes respectively [44]. For selected modes it is possible that the initial phase difference of excited and ground state displacements may consequently result in cancellation or apparent damping of observed motion. The on-resonance excitation and sign and magnitude of second order dispersion minimizes non-linear cross-sections of excited state absorption and stimulated emission [8,37,38,45]. While maximizing $S_0$ to $S_1$ population transfer, the intense femtosecond pulse also generates vibrational coherence. Vibrational coherence in the ground state arises

from four-wave mixing processes, is impulsive in nature and depends on the electronic dephasing time, the $S_1$ potential curvature and displacement, the pulse duration and vibrational dephasing, the pulse carrier frequency and sign and magnitude of dispersion [44,46,47]. Kumar et al. showed that for the generated ground state coherence for the case of on-resonance pumping, the impulse momentum is maximised and opposite in direction to the direction of the electron-nuclear coupling force, the phase becomes $\pi/2$ and the amplitude (the modulus of the complex displacement) is suppressed compared to near-resonance excitation [44]. The vibrational coherence generated in the ground state is thus 'hole-like' and at resonance generates a hole centred at equilibrium position (thus corresponding to $\cos(\pi/2)$) Linear response theory was used to show that the excited state vibrational coherence amplitude is generally not impulsive and depends on temperature and displacement [44]. In contrast to ground state coherence, the excited state coherence is 'particle-like' and thus must have a phase of either 0 or $\pi$ (the modulus of the complex excited state mode equals the displacement at time zero). Furthermore, positive second order dispersion further suppresses ground state coherence relative to excited state coherence [47,48], as was used in Pande et al. [12]. Therefore, while ground state contributions cannot be excluded for early delays, the experimental conditions were chosen to enhance selectively the contributions of excited state vibrational coherence as well as maximize the transfer to $S_1$.

Linear response theory of four-wave mixing typically represents the separate moments from cumulant expansions of the density operator, as shown by several authors in the past [46,49–52]. A very useful picture of the interaction caused by the pump pulse, when separated from a probe, represents the 'Wigner' phase space [53–55] which allows a semi-classical description of the ultrafast material response. An effective linear response theory was presented, that uses the 'doorway-window' picture to separate the pump and the probe interactions [56] which is

developed from the lineshape function [44]. Here, particular attention is paid to an estimate of the magnitude of the ground state vibrational coherence. Theory that treats the ground state and excited state coherence of a two-level system under resonant and off-resonant excitation is already a considerable problem [44,46–48,57]. Systems that additionally include ultrafast nonradiative surface crossing, such as for example myoglobin-CO [58], bacteriorhodopsin [46,59], PYP [60] and small photoswitching molecules [61] will also show vibrational coherence that is generated by non-Raman active coordinates. Kumar et al. [57] also developed formalisms based on Landau-Zener crossing formula to incorporate the coherence associated with rapid surface crossing. The application of the derived expressions are argued to be restricted to systems that have unity quantum yield [57]. In the case of the PYP the primary quantum yield is not precisely established but is relatively low, on the order of ~0.2 [8,17]. We therefore simplify the discussion to neglect in the first instance the crossing-generated coherence and discuss the magnitude of coherence that exists in the simple $S_0$-$S_1$ two-level system for delays shorter than ~500 fs.

While the derivation and theory is described in full detail elsewhere [44,57], a brief summary given below clarifies the methodology to calculate the wavepacket position Q and momentum P in Wigner phase space, which we extend and apply to the high power regime. The third order response is fully represented by the polarisation.

$$P_i(t,\tau) = \int_{-\infty}^{t} dt_3 \int_{-\infty}^{t_3} dt_2 \int_{-\infty}^{t_2} dt_1 \, \chi^{(3)}_{ijkl}(t, t_1, t_2, t_3) E_{bj}(t_3 - \tau) E_{ak}(t_2) E_{al}(t_1) \qquad (5)$$

Where $\chi^{(3)}_{ijkl}$ represents the third-order susceptibility. An effective first order susceptibility $\chi^{eff}_{ij}$ describes the nonstationary medium created by the pump interaction [49,50]. Kumar et al. [57] developed methods referred to as the ‘doorway picture’ which expands the density matrix in

orders of cumulant expansion. This approach is particularly useful for considering coherence contributions under conditions of pump-probe TR-SFX, as it allows an evaluation of magnitude of pump-induced motion under conditions that are currently used for TR-SFX

The Wigner phase space calculation depends firstly on the spectral line-shape and pulse width dependence of the population, which is calculated by taking the trace of the density operator to provide the (remaining) ground state $N_{\mathrm{g}}$ after the pump interaction. We can use the formalisms derived by Kumar et al. [44,57] in order to calculate the magnitude of the ground state and excited state coherence amplitude, respectively.

$$N_{\mathrm{g}} = 1 - \frac{\left|\mu_{\mathrm{ge}}\right|^2}{\pi\hbar^2}\int_{-\infty}^{\infty} d\omega \left|\tilde{E}(\omega)\right|^2 \Phi_I(\omega) \tag{6}$$

Where $\Phi_I(\omega)$ is the imaginary part of the complex line shape function.

$$\Phi_I(\omega) = i\int_0^{\infty} ds\, e^{i(\omega-\Omega_{00})s} e^{-\Gamma_{\mathrm{eg}}|s|} e^{-g(s)} \tag{7}$$

Kumar et al. show that in the cumulant expansion of the initial wavepacket position $\bar{Q}_g(0)$ of the ground state, the first moment is given as

$$\bar{Q}_{\mathrm{g}}(0) = -\frac{\left|\mu_{\mathrm{ge}}\right|^2 E_0^2(2\bar{n}+1)\Delta}{8\pi\hbar^2 N_{\mathrm{g}}} \times \int_0^{\infty} d\omega\, \tilde{G}_{\mathrm{p}}(\omega-\omega_c, -\omega_0)\hat{\Delta}\Phi_I(\omega) \tag{8}$$

Whereas the initial impulse momentum $\bar{P}_{\mathrm{g}}(0)$

$$\bar{P}_{\mathrm{g}}(0) = \frac{\left|\mu_{\mathrm{ge}}\right|^2 E_0^2\Delta}{8\pi\hbar^2 N_{\mathrm{g}}}\int_0^{\infty} d\omega\, \tilde{G}_p(\omega-\omega_c, -\omega_0)\hat{\Delta}\Phi_R(\omega) \tag{9}$$

Which uses a product spectral function

$$\tilde{G}_p(\omega, n\omega_0) = \tilde{G}(\omega)\tilde{G}(\omega + n\omega_0) \quad (10)$$

This result led to the very clear frequency dependent representation of the initial position and impulse momentum imparted on the remaining ground state population, developed from the line-shape function directly. The initial position Q and momentum P are given to be normalised by the remaining ground state population, $N_{\mathrm{g}}$. For weak pulses directly on resonance it is seen that the initial position is minimised, near zero, whereas the imparted impulse momentum is maximised and negative, thus opposite in direction to the restoring electron-nuclear force. The calculations further demonstrate that detuning from resonance generates initial position but generally reduces momentum. The complex coherence amplitude,$|A_{1\mathrm{g}}| = \sqrt{\left(Q_{\mathrm{g}}^2(0) + P_{\mathrm{g}}^2(0)\right)}$, which has phase $\Phi_{\mathrm{g}} = -\tan^{-1}[P_{\mathrm{g}0}/Q_{\mathrm{g}0}]$is taken as a measure of the ground state vibrational coherence magnitude.

A further visualisation of the ground state process plots the spectral ‘hole’ that is generated by the pulse. The figure 6 shows the theoretical line shape function and the resulting spectral hole after the interaction when the laser spectrum is placed at resonance for two different pulse lengths at several powers. It can be seen that in the case of the longer pulse a far more prominent spectral ‘hole’ is visible, while for the short pulse this effect is reduced.

The equations are given strictly for weak excitation, in which case the population is taken to be proportional to the intensity and the squared transition dipole. The convolution of the laser intensity spectrum and the absorption line shape is included in the spectral integral. For intense pulses the population is no longer linearly dependent on the intensity and cannot exceed population inversion. Formally, in order to treat intense optical pulses interacting with cross sections typical for pigments absorbing in the visible, a higher order expansion of the density

operator should be performed. However, this would also present a significant approximation, as the density operator used to derive the equations 6-10 are those for a two-level system, in which for instance population inversion is not possible and Rabi oscillations would occur for a higher order expansion. In practise, the PYP more likely acts as a three- or four-level system, depending on the pulse durations and excited state dynamics, potentially allowing population inversion. For the purpose of this contribution we wish to use linear response theory to demonstrate that 1) the magnitude of ground state coherence is comparable to that of excited state coherence, and 2) the ground state coherence may be manipulated using the carrier frequency and laser band-width. In order to use existing linear response theory we modify the weak-field expression for $N_{\mathrm{g}}$ (equation 6) to prevent negative values with the usual transformation of the product of cross section and intensity with the time dependent rate function. We thus calculate population for intense pulses according to

$$N_{\mathrm{g}} = \exp\left(-\frac{\left|\mu_{\mathrm{ge}}\right|^2 E_0^2}{4\pi\hbar^2}\int_0^\infty d\omega\, \tilde{G}^2(\omega-\omega_c)\Phi_I(\omega)\right) \tag{11}$$

$$N_{\mathrm{e}} = 1 - N_{\mathrm{g}} = 1 - \exp\left(-\frac{\left|\mu_{\mathrm{ge}}\right|^2 E_0^2}{4\pi\hbar^2}\int_0^\infty d\omega\, \tilde{G}^2(\omega-\omega_c)\Phi_I(\omega)\right) \tag{12}$$

With the above modification for intense excitation, the figure 7 calculates the initial position, impulse and amplitude as a function of power density. It should be pointed out that these calculations make a number of approximations. The equations are valid firstly in the impulsive approximation, when pulses are shorter than the vibrational period. Thus, the result is bandwidth limited to the 140 fs optical pulse duration used for pumping PYP crystals, which imposes the 3.15 THz experimental bandwidth limit. The stationary picture therefore also neglects chirp, electronic dephasing and Franck-Condon motion within the pulse duration [47,48]. The calculations indicate that for weak excitation directly on resonance the amplitude

of ground state coherence may be minimised and arise principally from the imparted momentum (figure 7). However, with intense pulses the on-resonant condition can generally not avoid the increased ground state coherence amplitude. The initial position $\bar{Q}_g(0)$ will increase as may be visualised in Wigner phase space: the 'hole' that the laser pulse creates in the ground state population will become significant and remaining population $N_g$ will decrease, thus increasing $\bar{Q}_g(0)$. Of course the initial momentum will continue to rise with increased intensity as well (figure 7). Calculations are not necessary to consider two boundary condition in which ground state coherence may be suppressed at high intensity. The first possibility is that the laser bandwidth is in excess of the spectroscopic line-width and the pulse is extremely short. In this case the broad spectrum bleaches all the nuclear coordinates to the same extent and no moving hole will be generated. An experimental report of such a condition has been made, reporting excited state coherence preferentially by using sub-5 fs pulses [59]. And secondly, with very long pulses the bandwidth similarly will of course not have the ability to generate a moving hole.

Finally, we consider an experimental scenario that may be possible in the future, which suppresses as much as possible the ground state coherence contributions by using extremely short pulses. A primary requirement is the development of much enhanced crystallographic sensitivity to detect photoinduced structure factor differences. One possibility to achieve higher sensitivity would be to exploit the high repetition rate of the European XFEL in order to collect many more pump-probe X-ray diffraction images. An alternative approach has been proposed to develop a split-beam probe-pump-probe measurement which could deliver superior and direct measurements of photoinduced structure factor differences [62]. Under conditions of significantly increased sensitivity, requirements for the optical pulse energy can be relaxed and shorter pulses could be considered. The following calculations for on-resonance

excitation conditions evaluate the ground state coherence magnitude by decreasing both the pulse duration and the energy.

For the excited state coherence the assumption is made that transfer to $S_1$ does not impart momentum [44]. Thus, the initial position $\bar{Q}_{\mathrm{e}}(0)$ gives the amplitude of the excited state vibrational coherence, whereas the initial phase can assume values of either 0 or π.

$$\bar{Q}_{\mathrm{e}}(0) = -\frac{\left|\mu_{\mathrm{ge}}\right|^2 E_0^2 \Delta}{4\pi\hbar N_{\mathrm{e}}} \int_0^{\infty} d\omega \tilde{G}_p(\omega - \omega_c, -\omega_0) \times \left[\Phi_I(\omega - \omega_0) - \bar{n}\hat{\Delta}\Phi_I(\omega)\right] \quad (13a)$$

$$\bar{P}_{\mathrm{e}}(0) = 0 \quad (13b)$$

The non-impulsive nature of the excited state coherence is discussed in contrast to ground state coherence that arises from four-wave mixing, Raman-active, processes and thus impart impulse momentum [44]. As before figure 8 shows calculations of the excited state initial position and total momentum using the same pulse conditions as those in figure 6 & 7. A comparison of the ground (figure 7) and excited (figure 8) state position moments suggests that through the use of shorter (larger bandwidth) pump pulses one can significantly reduce the ground state moment contribution without significantly reducing an excited state signal.

***5. Real-space amplitude of displacement of coherent vibrational modes***

The mode composition of vibrational coherences that are excited under our experimental conditions include low-frequency collective modes involving protein motion, which may be observed within the vibrational dephasing time. Displacements of high frequency modes in the fingerprint spectral region which correspond to chromophore vibrations are at the picometre level but cannot contribute to coherence with the previously reported experimental bandwidth

of 3.15 THz [12]. For example, a harmonic frequency calculation of the coumaric acid chromophore of PYP at the B3LYP/6-31+G(d) level retrieves a 1674 $cm^{-1}$ frequency for the C=C stretching mode together with a reduced mass of 6.14 $m_u$. Using the classical expression (equation 14) at 298 K temperature a value of $\sigma$=2 pm is calculated for the root mean square displacement. Both the frequency and the displacement are outside the presently achievable experimental bandwidth and experimental sensitivity, respectively [12].

However, low-frequency collective protein motions strongly contribute to the spectral density via the electron-phonon coupling. Hole-burning, Raman and fluorescence line narrowing spectroscopy demonstrate the strength of the electron-phonon coupling (vibronic) of the phonon-sideband peaking in the 20-50 $cm^{-1}$ region [63–65]. Typical vibronic coupling strengths in the spectral density for pigments embedded in proteins have Huang-Rhys factors on the order of ~0.5 as measured from the 'phonon-sideband' or 'Boson-peak' [63–65]. Low frequency collective modes are characterised by harmonic frequency calculation [66–68], molecular dynamics simulations and inelastic neutron scattering [69,70], which characterize low frequency modes at ~2 THz and below showing typical rms displacements of thermally activated low frequency modes at ~0.5 Å [71–75]. Earlier reported discrepancies between the frequencies and amplitudes of low frequency modes of proteins comparing molecular dynamics simulation and experiment (focussing on the temperature dependence of displacements from inelastic neutron scattering) have been argued to arise primarily from explicit representation of the molecular environment rather than presenting limitations of classical force fields [69].

The anisotropic Debye-Waller factor analysis from high resolution X-ray crystallography has been reported specifically for the case of the PYP [76]. While these measurements retrieved

ground state properties, a mode analysis of the displacements of the active site was possible. Based on the general literature of anisotropic Debye-Waller factor analysis of crystals given in many places [72,77–83] it is understood that vibrational displacement with amplitude > 0.1 Å must arise from very low frequency modes below 30 $cm^{-1}$ generally. Individual low frequency normal modes contributing to the spectral density have amplitudes smaller than the average, summed, 0.5 Å rms displacement, while those below 30 $cm^{-1}$ contribute most to the overall rms displacement [84]. It should be pointed out that many studies of vibrational displacements of proteins at room temperature, including treatments of the Debye-Waller factor [77,78,82,85] and even at low temperatures [69] write the Classical expression for the root mean square displacement as the second moment of the Gaussian distribution, as

$$\langle \sigma^2 \rangle = \frac{k_B T}{\mu \omega_0^2} \tag{14}$$

Where μ is the reduced mass of the oscillator with natural frequency $\omega_0$. The above expression is taken as the high temperature limit of the displacement of the quantum oscillator [80,83,86].

$$\langle \sigma^2 \rangle = \frac{\hbar}{2\mu\omega_0} \coth\left(\frac{\hbar\omega_0}{2k_B T}\right) = \frac{\hbar}{2\mu\omega_0}[2\bar{n} + 1] \tag{15}$$

With the occupation number

$$\bar{n} = \left[e^{\hbar\omega_0/k_B T} - 1\right]^{-1} \tag{16}$$

Even at 298 K, the classical expression systematically underestimates the displacement particularly of high frequency modes $\hbar\omega_0 \gg k_B T$that are in the ground state. For instance the quantised expression retrieves a value of σ= 4 pm for the above mentioned chromophore C=C mode, twice the value that is calculated using the classical expression. Also for low frequencies the classical expression underestimates the displacement by 10% already at 250 $cm^{-1}$

frequency, at 298 K. Nevertheless, since generally the very low frequency modes $\hbar\omega_0 < 30$ cm$^{-1}$ dominate the amplitudes of the anisotropic Debye-Waller factors, the classical approach is a reasonable approximation at ambient or higher temperature for the analysis of static X-ray crystallographic data.

For illustration, a harmonic frequency calculation of PYP using the Amber force field and the Gaussian 09 package [87] evaluates the frequency dependence of the root mean square displacement at 298 K (figure 9). The calculated reduced masses printed by the Gaussian program are computed by normalisation via the Cartesian displacement as outlined in Frisch et al. [87]. The figure demonstrates that vibrational displacements below 1500 cm$^{-1}$ frequency are calculated to be ≥0.1 Å. Characteristic fingerprint region vibrations in the 1200-1700 cm$^{-1}$ spectral region are associated with increased reduced masses resulting in smaller RMS displacements (figure 9).

An interesting point regarding very low frequency modes calculated here (figure 9) is that about 70 modes below 30 cm$^{-1}$ have RMS displacement values above 1 Å, which are likely overestimated. For instance, an analysis of the anisotropic B-factors from high resolution X-ray diffraction of PYP specifically and other proteins in general indicates limits in the 0.5-1 Å. It should be noted that for these low frequencies at room temperature differences between the quantised and the classical expression usually employed in the B-factor analysis method, are in fact negligible. Figure 9 however illustrates that the displacement of modes in the 500-1500 cm$^{-1}$ region involves displacements at the 10 pm level which could potentially be resolved with time resolved crystallographic detection if very good sensitivity is obtained. Because of the generally increased reduced mass, modes in the interesting 1500-1750 cm$^{-1}$ region should typically involve smaller displacements (figure 9). The result motivates the future development of increased band-width and increased signal-to-noise of detection of photoinduced differences

to develop the crystallographic equivalent of an impulsive Raman spectroscopy measurement of vibrational coherence.

Details of the calculation of the reduced mass that affect the rms displacement of low frequency modes using the harmonic approximation in the Gaussian program concern the normalisation of the Cartesian displacements

$$\mu_i = \left( \sum_k^{3N} I^2_{\mathrm{cart};k,i} \right)^{-1} = \left( \sum_k^{3N} \left( \frac{I_{\mathrm{mwc};\,k,i}}{\sqrt{m_k}} \right)^2 \right)^{-1} \tag{17}$$

The harmonic approximation will thus the underestimate of the mass weighted coordinate ($I_{\mathrm{mwc}}$) for the soft low frequency modes. Investigations of higher order anharmonicity arrived at very good agreement between frequency calculations of low frequency modes and experimental observables including the Debye-Waller terms [67,68].

The harmonic calculation for PYP nevertheless demonstrates that there is motivation to further develop both the experimental bandwidth and the sensitivity (SNR) for TR-SFX experiments. Future high repetition rate TR-SFX experiments at the European XFEL may achieve greater sensitivity to coherent vibrational displacement, which at the 0.1 Å level may be achievable together with enhanced experimental bandwidth, possibly even employing few-femtosecond optical pulses. An alternative strategy has been proposed to employ a non-colinear split beam 'probe-pump-probe' may allow direct measurement of photoinduced structure factor differences with enhanced sensitivity potentially allowing high frequency and small amplitude vibrational coherence to be observed [62].

### *6. Conclusions and outlook*

We have discussed the ramifications of the recently employed experimental regime in order to achieve a femtosecond time resolved TR-SFX experiment of protein dynamics [12]. We have primarily considered how the power and band-width causes selection of nuclear coordinates and furthermore drives significant non-linear processes including stimulated emission, excited state absorption, photoionisation and four-wave mixing. Well-developed formalism from the Raman literature can be applied to the high field regime with appropriate modifications, and are presented as an approximation, providing the dominating contributions – e.g. taking the first moment from the cumulant expansion of the density operator. The calculations of the magnitude of ground state and excited state vibrational coherence demonstrate that for typical conditions for femtosecond time resolved TR-SFX both will be generated and are expected to have significant amplitude. Also, the typical amplitudes are likely to be comparable, but is should be emphasized that the two types of resulting motion will have different initial phases. A pump-probe measurement of real-space displacement will therefore reflect a complicated signal that must result from the addition of the two types of motions which will generally have modified frequencies and mode compositions as well as phase. The assignment of $S_1$-dominated Franck-Condon motion to delays smaller than 550 fs in PYP TR-SFX data is a proposal based primarily on the magnitude of displacement seen, but the contributions of vibrational coherences are expected. Future approaches will use optical control to manipulate the contributions to femtosecond motion. This review has provided motivation for using experimental methods that can manipulate the coherent motions, these include the optical parameters of band-width, intensity, spectral phase, carrier frequency (detuning) and potentially also pulse complexity. We suggest that methods from high-field coherent control will not only aid the manipulation of population transfer but also allow the manipulation of coherence contributions. We thus anticipate the future high repetition rate combined with few-

femtosecond capabilities of XFEL instruments to provide experimental access to high frequency, low amplitude vibrational coherence in protein crystals.

***Bibliography***

[1] Y. O. Jung, J. H. Lee, J. Kim, M. Schmidt, K. Moffat, V. Šrajer, and H. Ihee, Nat. Chem. **5**, 212 (2013).
[2] F. Schotte, H. S. Cho, V. R. I. Kaila, H. Kamikubo, N. Dashdorj, E. R. Henry, T. J. Graber, R. Henning, M. Wulff, G. Hummer, M. Kataoka, and P. A. Anfinrud, Proc. Natl. Acad. Sci. U. S. A. **109**, 19256 (2012).
[3] F. Schotte, M. Lim, T. A. Jackson, A. V. Smirnov, J. Soman, J. S. Olson, G. N. Phillips, M. Wulff, and P. A. Anfinrud, Science **300**, 1944 (2003).
[4] B. Perman, V. Šrajer, Z. Ren, T. Teng, C. Pradervand, T. Ursby, D. Bourgeois, F. Schotte, M. Wulff, R. Kort, K. Hellingwerf, and K. Moffat, Science **279**, 1946 (1998).
[5] Z. Ren, B. Perman, V. Šrajer, T.-Y. Teng, C. Pradervand, D. Bourgeois, F. Schotte, T. Ursby, R. Kort, M. Wulff, and K. Moffat, Biochemistry **40**, 13788 (2001).
[6] K. Moffat, Acta Crystallogr. Sect. A Found. Crystallogr. **54**, 833 (1998).
[7] H. Ihee, S. Rajagopal, V. Šrajer, R. Pahl, S. Anderson, M. Schmidt, F. Schotte, P. A. Anfinrud, M. Wulff, and K. Moffat, Proc. Natl. Acad. Sci. U. S. A. **102**, 7145 (2005).
[8] C. N. Lincoln, A. E. Fitzpatrick, and J. J. van Thor, Phys. Chem. Chem. Phys. **14**, 15752 (2012).
[9] Y. O. Jung, J. H. Lee, J. Kim, M. Schmidt, K. Moffat, V. Šrajer, and H. Ihee, Nat. Chem. **6**, 259 (2014).
[10] V. R. I. Kaila, F. Schotte, H. S. Cho, G. Hummer, and P. A. Anfinrud, Nat. Chem. **6**, 258 (2014).
[11] J. Tenboer, S. Basu, N. Zatsepin, K. Pande, D. Milathianaki, M. Frank, M. Hunter, S. Boutet, G. J. Williams, J. E. Koglin, D. Oberthuer, M. Heymann, C. Kupitz, C. Conrad, J. Coe, S. Roy-Chowdhury, U. Weierstall, D. James, D. Wang, T. Grant, A. Barty, O. Yefanov, J. Scales, C. Gati, C. Seuring, V. Srajer, R. Henning, P. Schwander, R. Fromme, A. Ourmazd, K. Moffat, J. J. Van Thor, J. C. H. Spence, P. Fromme, H. N. Chapman, and M. Schmidt, Science **346**, 1242 (2014).
[12] K. Pande, C. D. M. Hutchison, G. Groenhof, A. Aquila, J. S. Robinson, J. Tenboer, S. Basu, D. P. DePonte, M. Liang, T. A. White, N. Zatsepin, O. Yefanov, D. Morozov, D. Oberthuer, C. Gati, G. Subramanian, D. James, Y. Zhao, J. Koralek, J. Brayshaw, C. Kupitz, C. Conrad, S. Roy-Chowdhury, J. Coe, M. Metz, P. L. Xavier, T. D. Grant, J. E. Koglin, G. Ketawala, R. Fromme, V. Srajer, R. Henning, J. C. H. Spence, A. Ourmazd, P. Schwander, U. Weierstall, M. Frank, P. Fromme, A. Barty, H. N. Chapman, K. Moffat, J. J. van Thor, and M. Schmidt, Submitted to Science (n.d.).
[13] A. Warshel, Nature **260**, 679 (1976).
[14] A. Barty, C. Caleman, A. Aquila, N. Timneanu, L. Lomb, T. A. White, J. Andreasson, D. Arnlund, S. Bajt, T. R. M. Barends, M. Barthelmess, M. J. Bogan, C. Bostedt, J. D. Bozek, R. Coffee, N. Coppola, J. Davidsson, D. P. Deponte, R. B. Doak, T. Ekeberg, V. Elser, S. W. Epp, B. Erk, H. Fleckenstein, L. Foucar, P. Fromme, H. Graafsma, L. Gumprecht, J. Hajdu, C. Y. Hampton, R. Hartmann, A. Hartmann, G. Hauser, H. Hirsemann, P. Holl, M. S. Hunter, L. Johansson, S. Kassemeyer, N. Kimmel, R. A. Kirian, M. Liang, F. R. N. C. Maia, E. Malmerberg, S. Marchesini, A. V. Martin, K. Nass, R. Neutze, C. Reich, D. Rolles, B. Rudek, A. Rudenko, H. Scott, I. Schlichting, J. Schulz, M. M. Seibert, R. L. Shoeman, R. G. Sierra, H. Soltau, J. C. H. Spence, F. Stellato, S. Stern, L. Strüder, J. Ullrich, X. Wang, G. Weidenspointner, U. Weierstall, C. B. Wunderer, and H. N. Chapman, Nat.

Photonics **6**, 35 (2012).
[15] L. Lomb, T. R. M. Barends, S. Kassemeyer, A. Aquila, S. W. Epp, B. Erk, L. Foucar, R. Hartmann, B. Rudek, D. Rolles, A. Rudenko, R. L. Shoeman, J. Andreasson, S. Bajt, M. Barthelmess, A. Barty, M. J. Bogan, C. Bostedt, J. D. Bozek, C. Caleman, R. Coffee, N. Coppola, D. P. Deponte, R. B. Doak, T. Ekeberg, H. Fleckenstein, P. Fromme, M. Gebhardt, H. Graafsma, L. Gumprecht, C. Y. Hampton, A. Hartmann, G. Hauser, H. Hirsemann, P. Holl, J. M. Holton, M. S. Hunter, W. Kabsch, N. Kimmel, R. A. Kirian, M. Liang, F. R. N. C. Maia, A. Meinhart, S. Marchesini, A. V. Martin, K. Nass, C. Reich, J. Schulz, M. M. Seibert, R. Sierra, H. Soltau, J. C. H. Spence, J. Steinbrener, F. Stellato, S. Stern, N. Timneanu, X. Wang, G. Weidenspointner, U. Weierstall, T. A. White, C. Wunderer, H. N. Chapman, J. Ullrich, L. Str??der, and I. Schlichting, Phys. Rev. B - Condens. Matter Mater. Phys. **84**, 214111 (2011).
[16] K. Nass, L. Foucar, T. R. M. Barends, E. Hartmann, S. Botha, R. L. Shoeman, R. B. Doak, R. Alonso-Mori, A. Aquila, S. Bajt, A. Barty, R. Bean, K. R. Beyerlein, M. Bublitz, N. Drachmann, J. Gregersen, H. O. Jönsson, W. Kabsch, S. Kassemeyer, J. E. Koglin, M. Krumrey, D. Mattle, M. Messerschmidt, P. Nissen, L. Reinhard, O. Sitsel, D. Sokaras, G. J. Williams, S. Hau-Riege, N. Timneanu, C. Caleman, H. N. Chapman, S. Boutet, and I. Schlichting, J. Synchrotron Radiat. **22**, 225 (2015).
[17] C. D. M. Hutchison, M. Kaucikas, J. Tenboer, C. Kupitz, K. Moffat, M. Schmidt, and J. J. van Thor, Chem. Phys. Lett. **654**, 63 (2016).
[18] S. Anderson, S. Crosson, and K. Moffat, Acta Crystallogr. Sect. D Biol. Crystallogr. **60**, 1008 (2004).
[19] L. J. G. W. van Wilderen, M. A. van der Horst, I. H. M. van Stokkum, K. J. Hellingwerf, R. van Grondelle, and M. L. Groot, Proc. Natl. Acad. Sci. **103**, 15050 (2006).
[20] R. Nakamura, N. Hamada, H. Ichida, F. Tokunaga, and Y. Kanematsu, J. Chem. Phys. **127**, 215102 (2007).
[21] H. Chosrowjan, N. Mataga, N. Nakashima, Y. Imamoto, and F. Tokunaga, Chem. Phys. Lett. **270**, 267 (1997).
[22] M. Vengris, M. A. van der Horst, G. Zgrablić, I. H. M. van Stokkum, S. Haacke, M. Chergui, K. J. Hellingwerf, R. van Grondelle, and D. S. Larsen, Biophys. J. **87**, 1848 (2004).
[23] D. S. Larsen, I. H. M. van Stokkum, M. Vengris, M. A. van der Horst, F. L. de Weerd, K. J. Hellingwerf, and R. van Grondelle, Biophys. J. **87**, 1858 (2004).
[24] K. D. Rector and M. D. Fayer, Laser Chem. **19**, 19 (1999).
[25] N. Mataga, H. Chosrowjan, Y. Shibata, Y. Imamoto, M. Kataoka, and F. Tokunaga, Chem. Phys. Lett. **352**, 220 (2002).
[26] H. Chosrowjan, S. Taniguchi, N. Mataga, M. Unno, S. Yamauchi, N. Hamada, M. Kumauchi, and F. Tokunaga, J. Phys. Chem. B **108**, 2686 (2004).
[27] K. J. Hellingwerf, J. Hendriks, and T. Gensch, J. Phys. Chem. A **107**, 1082 (2003).
[28] P. J. M. Johnson, A. Halpin, T. Morizumi, V. I. Prokhorenko, O. P. Ernst, and R. J. D. Miller, Nat. Chem. **7**, 980 (2015).
[29] A. D. Stahl, M. Hospes, K. Singhal, I. van Stokkum, R. van Grondelle, M. L. Groot, and K. J. Hellingwerf, Biophys. J. **101**, 1184 (2011).
[30] D. S. Larsen and R. van Grondelle, ChemPhysChem **6**, 828 (2005).
[31] M. Creelman, M. Kumauchi, W. D. Hoff, and R. A. Mathies, J. Phys. Chem. B **118**, 659 (2014).
[32] S. Yeremenko, I. H. M. van Stokkum, K. Moffat, and K. J. Hellingwerf, Biophys. J. **90**, 4224 (2006).
[33] M. Shapiro and P. Brumer, J. Chem. Phys. **84**, 4103 (1986).
[34] P. Brumer and M. Shapiro, Annu. Rev. Phys. Chem. **43**, 257 (1992).
[35] R. Kosloff, S. A. Rice, P. Gaspard, S. Tersigni, and D. J. Tannor, Chem. Phys. **139**, 201

(1989).
[36] S. H. Tersigni, P. Gaspard, and S. A. Rice, J. Chem. Phys. **93**, 1670 (1990).
[37] D. J. Tannor, R. Kosloff, and S. A. Rice, J. Chem. Phys. **85**, 5805 (1986).
[38] S. Ruhman and R. Kosloff, J. Opt. Soc. Am. B **7**, 1748 (1990).
[39] I. Pastirk, E. J. Brown, Q. Zhang, and M. Dantus, J. Chem. Phys. **108**, 4375 (1998).
[40] D. Sharma, A. Huijser, J. Savolainen, G. Steen, and J. L. Herek, Faraday Discuss. **163**, 433 (2013).
[41] J. T. Sage, Y. Zhang, J. McGeehan, R. B. G. Ravelli, M. Weik, and J. J. Van Thor, Biochim. Biophys. Acta - Proteins Proteomics **1814**, 760 (2011).
[42] K. Ng, E. D. Getzoff, and K. Moffat, Biochemistry **34**, 879 (1995).
[43] M. F. Perutz and J. M. Mitchison, Nature **166**, 677 (1950).
[44] A. T. N. Kumar, F. Rosca, A. Widom, and P. M. Champion, J. Chem. Phys. **114**, 6795 (2001).
[45] J. Manz, H. Naundorf, K. Yamashita, and Y. Zhao, J. Chem. Phys. **113**, 8969 (2000).
[46] W T Pollard and and R. A. Mathies, Annu. Rev. Phys. Chem. **43**, 497 (1992).
[47] A. Wand, S. Kallush, O. Shoshanim, O. Bismuth, R. Kosloff, and S. Ruhman, Phys. Chem. Chem. Phys. **12**, 2149 (2010).
[48] C. J. Bardeen, Q. Wang, and C. V. Shank, Phys. Rev. Lett. **75**, 3410 (1995).
[49] W. T. Pollard, S. L. Dexheimer, Q. Wang, L. A. Peteanu, C. V. Shank, and R. A. Mathies, J. Phys. Chem. **96**, 6147 (1992).
[50] B. Fain and S. H. Lin, Chem. Phys. **161**, 515 (1992).
[51] B. Fain, S. H. Lin, and V. Khidekel, Phys. Rev. A **47**, 3222 (1993).
[52] B. Fain and S. H. Lin, Chem. Phys. Lett. **207**, 287 (1993).
[53] Y. J. Yan, L. E. Fried, and S. Mukamel, J. Phys. Chem. **93**, 8149 (1989).
[54] Y. J. Yan and S. Mukamel, Phys. Rev. A **41**, 6485 (1990).
[55] S. Mukamel, Annu. Rev. Phys. Chem. **41**, 647 (1990).
[56] S. Mukamel, *Principles of Nonlinear Optical Spectroscopy*, New Ed edi (Oxford University Press, 1995).
[57] A. T. N. Kumar, F. Rosca, A. Widom, and P. M. Champion, J. Chem. Phys. **114**, 701 (2001).
[58] R. J. Miller, Annu. Rev. Phys. Chem. **42**, 581 (1991).
[59] T. Kobayashi, T. Saito, and H. Ohtani, in *Nature* (2001), pp. 531–534.
[60] J. Liu, K. Okamura, Y. Kida, T. Teramoto, and T. Kobayashi, Opt. Express **18**, 20645 (2010).
[61] J. Léonard, J. Briand, S. Fusi, V. Zanirato, M. Olivucci, and S. Haacke, New J. Phys. **15**, 105022 (2013).
[62] J. J. van Thor and A. Madsen, Struct. Dyn. **2**, 14102 (2015).
[63] J. Pieper, K.-D. Irrgang, M. Rätsep, J. Voigt, G. Renger, and G. J. Small, Photochem. Photobiol. **71**, 574 (2000).
[64] M. Rätsep, J. Pieper, K.-D. Irrgang, and A. Freiberg, J. Phys. Chem. B **112**, 110 (2008).
[65] K. G. Brown, S. C. Erfurth, E. W. Small, and W. L. Peticolas, Proc. Natl. Acad. Sci. U. S. A. **69**, 1467 (1972).
[66] L. M. Thompson, A. Lasoroski, P. M. Champion, J. T. Sage, M. J. Frisch, J. J. van Thor, and M. J. Bearpark, J. Chem. Theory Comput. **10**, 751 (2014).
[67] A. E. Roitberg, R. B. Gerber, and M. A. Ratner, J. Phys. Chem. B **101**, 1700 (1997).
[68] A. Roitberg, R. B. Gerber, R. Elber, and M. A. Ratner, Science **268**, 1319 (1995).
[69] M. Tarek, G. J. Martyna, and D. J. Tobias, J. Am. Chem. Soc. **122**, 10450 (2000).
[70] D. Vural, L. Hong, J. C. Smith, and H. R. Glyde, Phys. Rev. E **88**, 52706 (2013).
[71] B. Brooks and M. Karplus, Proc. Natl. Acad. Sci. **80**, 6571 (1983).
[72] G A Petsko and and D. Ringe, Annu. Rev. Biophys. Bioeng. **13**, 331 (1984).

[73] W. Doster, S. Cusack, and W. Petry, Phys. Rev. Lett. **65**, 1080 (1990).
[74] J. Fitter, Biophys. J. **76**, 1034 (1999).
[75] H. Leyser, W. Doster, and M. Diehl, Phys. Rev. Lett. **82**, 2987 (1999).
[76] E. D. Getzoff, K. N. Gutwin, and U. K. Genick, Nat. Struct. Mol. Biol. **10**, 663 (2003).
[77] A. Kitao and N. Go, Curr. Opin. Struct. Biol. **9**, 164 (1999).
[78] A. Kidera, K. Inaka, M. Matsushima, and N. Gō, J. Mol. Biol. **225**, 477 (1992).
[79] B. T. M. Willis and G. S. Pawley, Acta Crystallogr. Sect. A Cryst. Physics, Diffraction, Theor. Gen. Crystallogr. **26**, 254 (1970).
[80] A. W. Hewat, J. Phys. C Solid State Phys. **5**, 1309 (1972).
[81] T. Ichiye and M. Karplus, Proteins Struct. Funct. Bioinforma. **2**, 236 (1987).
[82] W. F. Kuhs, Acta Crystallogr. Sect. A Found. Crystallogr. **48**, 80 (1992).
[83] J. D. Dunitz, E. F. Maverick, and K. N. Trueblood, Angew. Chemie Int. Ed. English **27**, 880 (1988).
[84] M. Levitt, C. Sander, and P. S. Stern, J. Mol. Biol. **181**, 423 (1985).
[85] G. Zaccai, Science **288**, 1604 (2000).
[86] A. A. Maradudin, E. W. Montroll, and G. H. Weiss, *Theory of Lattice Dynamics in the Harmonic Approximatione* (Academic Press, New York, 1963).
[87] M. J. Frisch, G. W. Trucks, H. B. Schlegel, G. E. Scuseria, M. A. Robb, J. R. Cheeseman, G. Scalmani, V. Barone, B. Mennucci, G. A. Petersson, H. Nakatsuji, M. Caricato, X. Li, H. P. Hratchian, A. F. Izmaylov, J. Bloino, G. Zheng, J. L. Sonnenberg, M. Hada, M. Ehara, K. Toyota, R. Fukuda, J. Hasegawa, M. Ishida, T. Nakajima, Y. Honda, O. Kitao, H. Nakai, T. Vreven, J. A. Montgomery Jr., J. E. Peralta, F. Ogliaro, M. J. Bearpark, J. Heyd, E. N. Brothers, K. N. Kudin, V. N. Staroverov, R. Kobayashi, J. Normand, K. Raghavachari, A. P. Rendell, J. C. Burant, S. S. Iyengar, J. Tomasi, M. Cossi, N. Rega, N. J. Millam, M. Klene, J. E. Knox, J. B. Cross, V. Bakken, C. Adamo, J. Jaramillo, R. Gomperts, R. E. Stratmann, O. Yazyev, A. J. Austin, R. Cammi, C. Pomelli, J. W. Ochterski, R. L. Martin, K. Morokuma, V. G. Zakrzewski, G. A. Voth, P. Salvador, J. J. Dannenberg, S. Dapprich, A. D. Daniels, Ö. Farkas, J. B. Foresman, J. V. Ortiz, J. Cioslowski, and D. J. Fox, (2009).
[88] G. E. O. Borgstahl, D. R. Williams, and E. D. Getzoff, Biochemistry **34**, 6278 (1995).

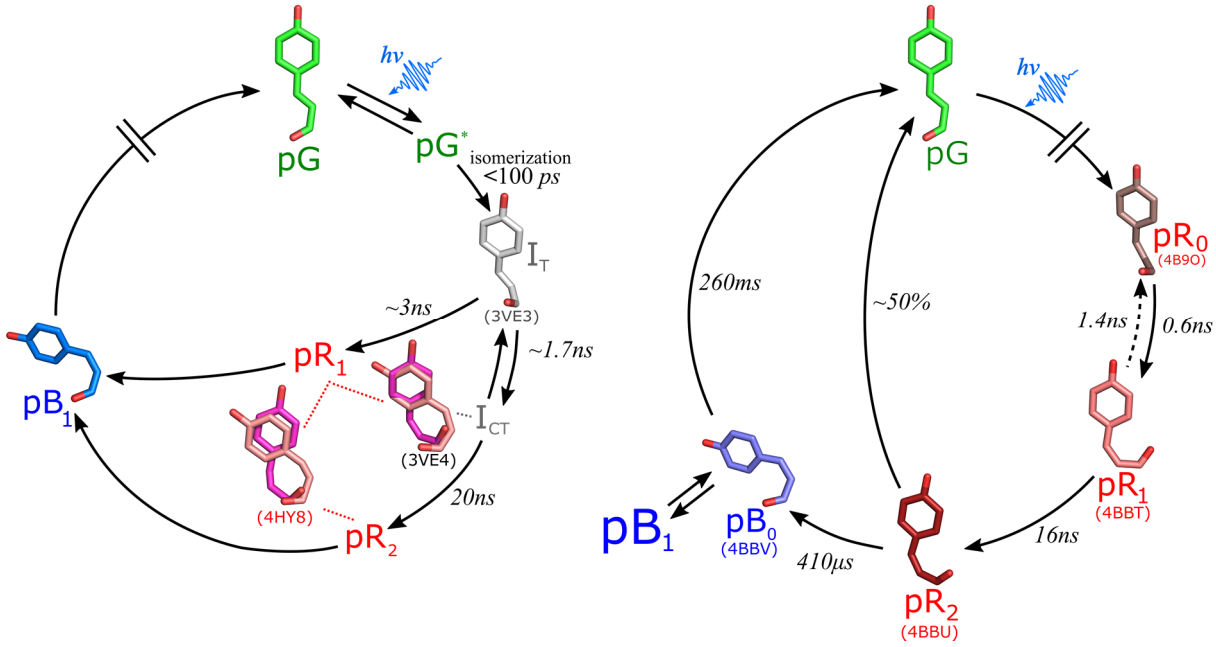


*Figure 1: Reaction schemes from TR-Laue studies (a) Jung et al.* [1] *and (b) Schotte et al.* [2] *of the PYP. The structures depicted for Jung are their ESRF/ID09B results which had better* $R_{free}$.

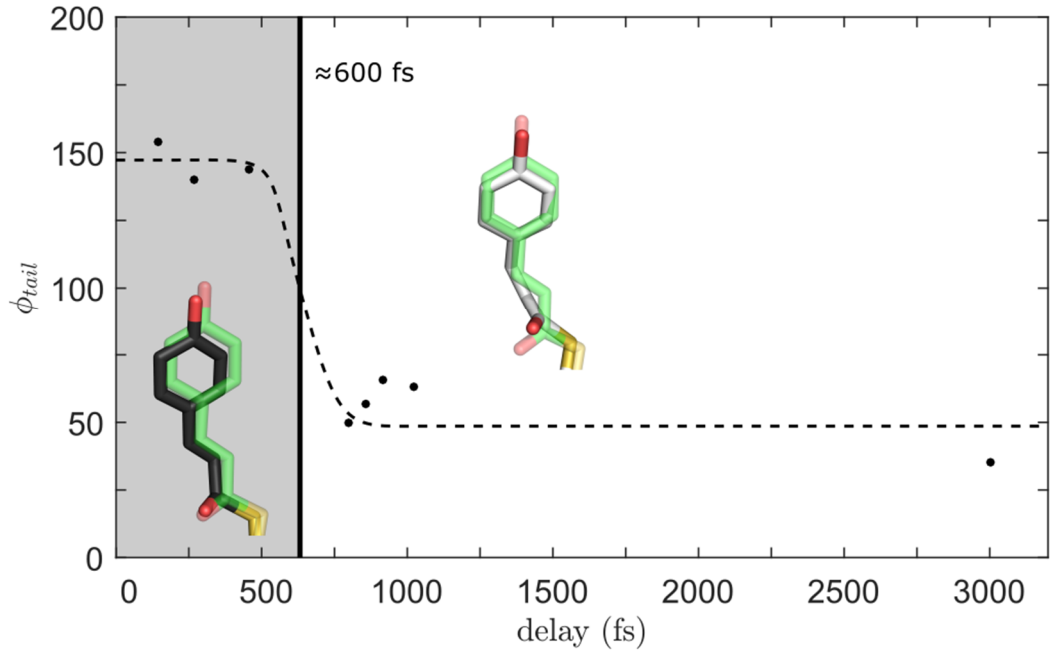


*Figure 2: PYP chromophore dihedral angle($\phi_{tail}$) against time after excitation from Pande et al.* [12]. *The transition between trans and cis chromophore structures is seen at ~600 fs. Refined chromophore structures (inserted) for the ~300 fs (black) and 3 ps (white) are shown compared the un-illuminated structure (transparent green).*

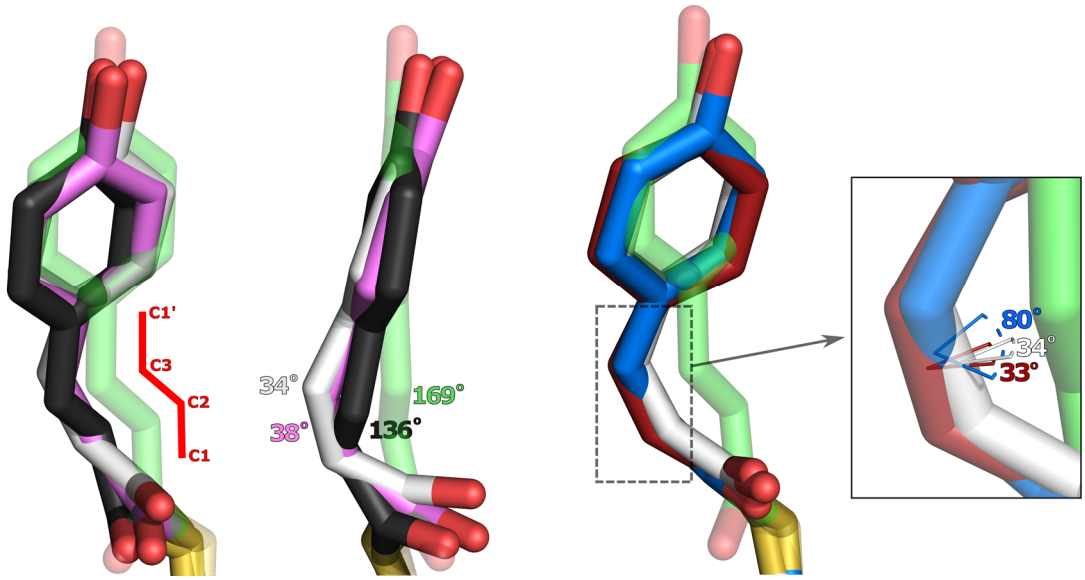


*Figure 3: Chromophore structures from (a) TR-SFX results from Pande et al.* [12] *at different time points, 269 fs (black), 940 fs (pink) and 3 ps (white) both face and side on. The dihedral angle of the chromophore tail($\phi_{tail}$) is shown by the red line. The values of $\phi_{tail}$ are labels of each structure are labelled in the side on view. (b) a comparison of the 3 ps time point, $I_T$ from Jung et al. (blue) and $pR_0$ from Schotte et al.* [2] *(dark red). Inset highlights the how the dihedral angle of the 3 ps is much closer to $pR_0$ than $I_T$. For reference the high resolution of the ground state (transparent green) from Anderson et al.* [18] *(pdb:1OT9) is also shown.*

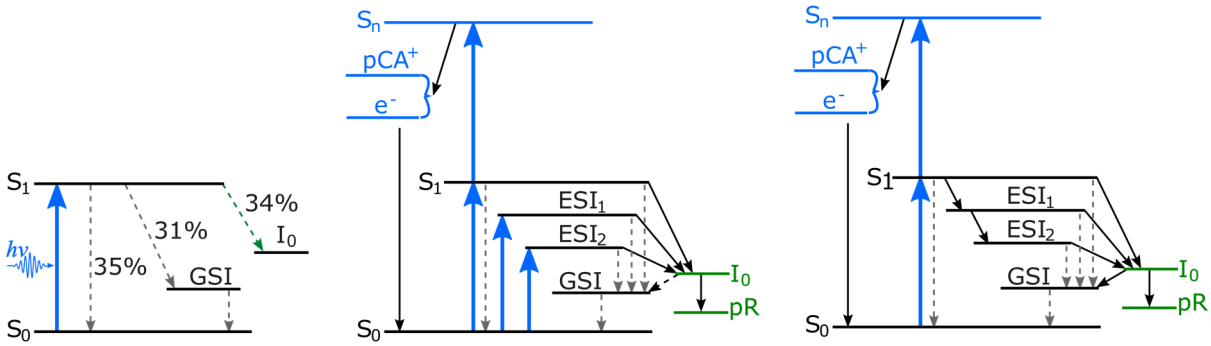


*Figure 4: Comparison of schemes for primary photochemical reaction of PYP. (a) General scheme from Stahl et al.* [29], *(b) Inhomogeneous and (c) Homogenous model for multiphasic dynamics of PYP transient absorption discussed in Larsen et al.* [23].

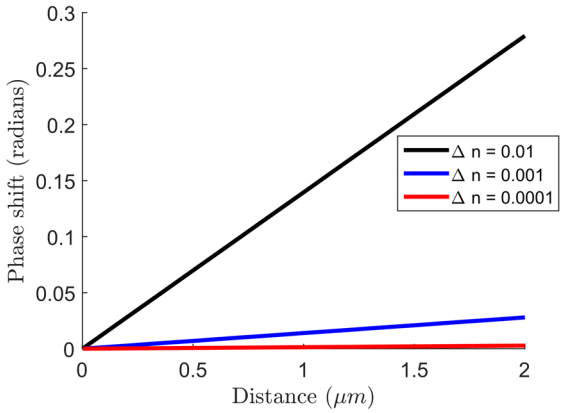


*Figure 5: Calculated maximum phase shift between two components of a beam propagating through a crystal with various levels of intrinsic bifringence (Δn).*

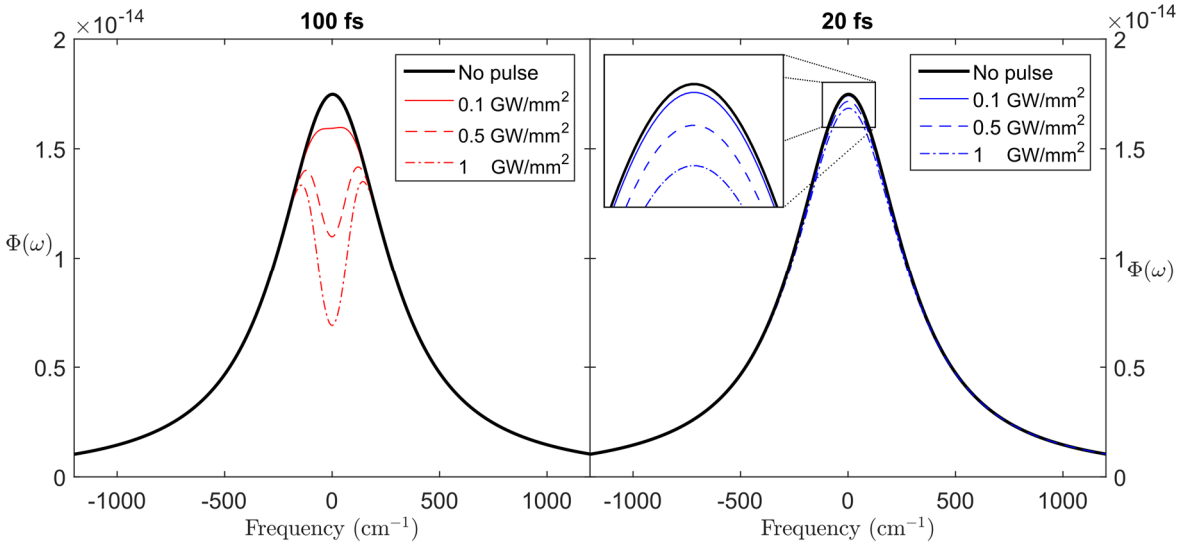


*Figure 6: Calculations of the 'spectral hole' created by excitation from a (a) 100 fs & (b) 20 fs pulses for various pulse energies. It can be seen that the extent of the localised spectral hole is inversely proportional to the pulse length.*

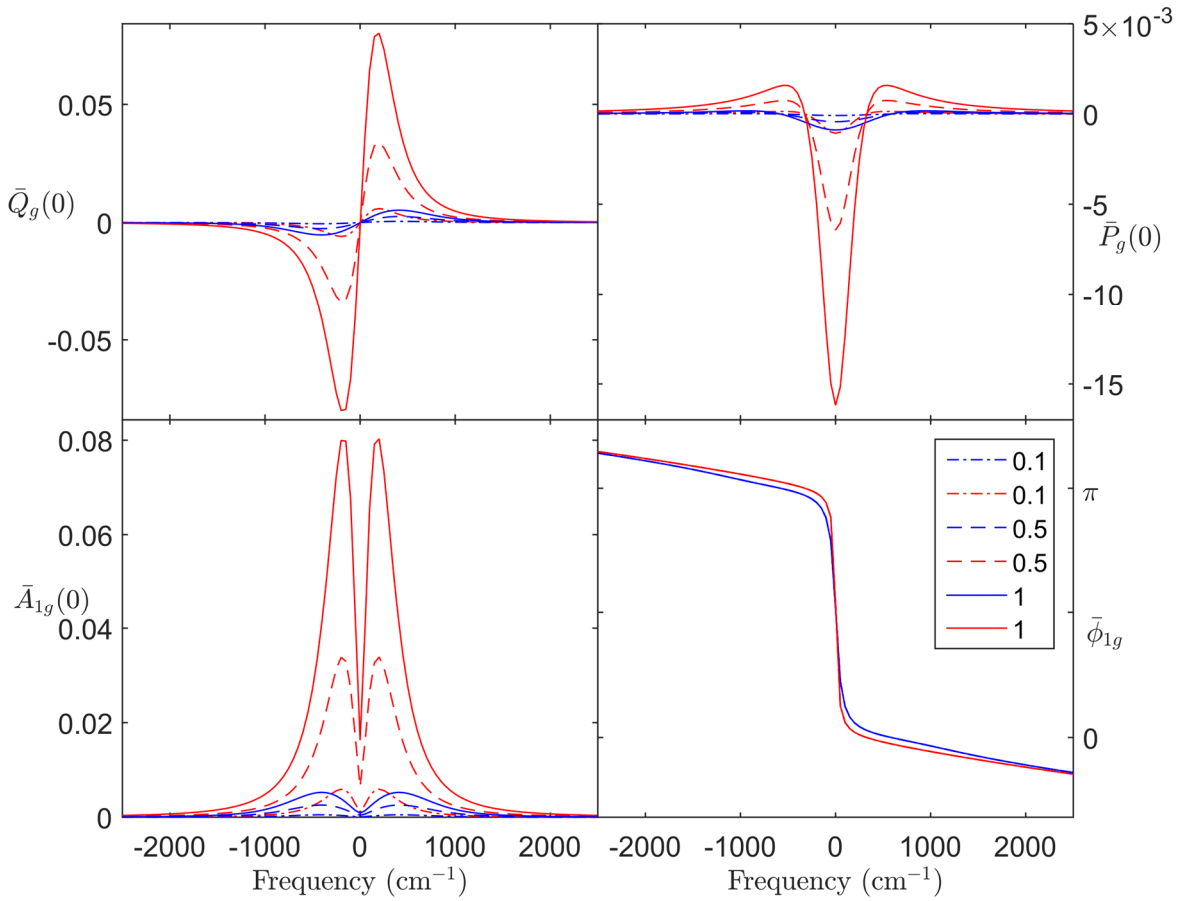


*Figure 7: Calculations of the ground state position Q, momentum P, total moment A and the phase for a 50cm$^{-1}$ mode for various pulse intensities. Excitation by a 20 fs (blue) and 100 fs (red) pulse are shown in red and blue respectively. Intensities are shown in GW/mm$^2$. In the case of 20 fs it can be seen that the magnitude of the moments in significantly reduced compared to the 100 fs.*

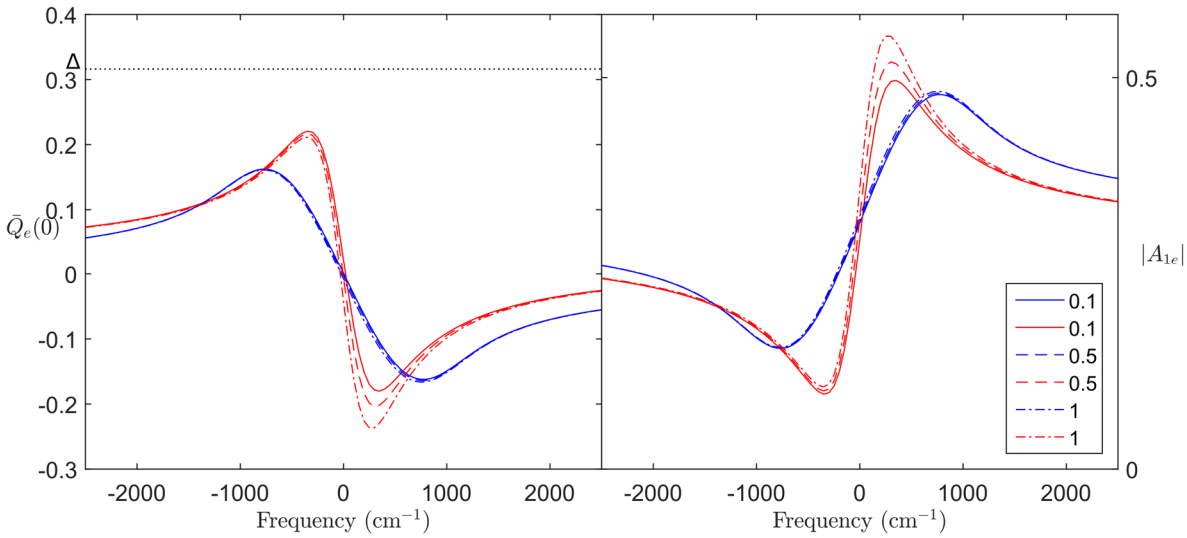


*Figure 8: Intensity dependence or the positional (left) and total (right) excited state moments for a 50 cm$^{-1}$mode. Excitation from a 20 fs (blue) and 100 fs (red) for various intensities in GW/mm$^2$. The equilibrium position (Δ) is shown as a black dotted line.*

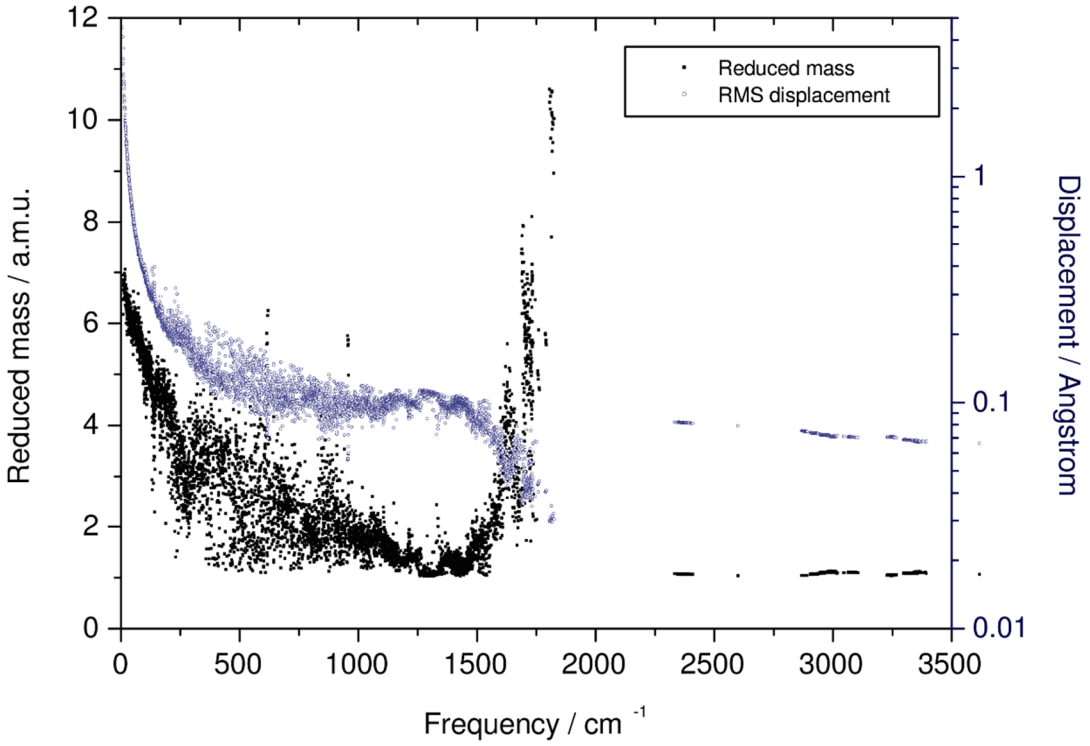


*Figure 9: The reduced masses (black) and calculated RMS displacement values (s/Å) of vibrational modes at room temperature for a harmonic frequency calculation of the PYP using protein and water coordinates from 2PHY pdb* [88]*. The RMS displacements are calculated using the quantum oscillator expression (equation 17), and are plotted as log to highlight the behaviour of low frequency modes < 30 cm$^{-1}$.*